OPEN ACCESS

University of BRISTOL

Armstrong, J. P. K., Burke, M., Carter, B. M., Davis, S. A., & Perriman, A. W. (2016). 3D Bioprinting Using a Templated Porous Bioink. Advanced Healthcare Materials, 5(14), 1724-1730. DOI: 10.1002/adhm.201600022

Publisher's PDF, also known as Version of record

Link to published version (if available):
10.1002/adhm.201600022

Link to publication record in Explore Bristol Research
PDF-document

University of Bristol - Explore Bristol Research
General rights

3D Bioprinting Using a Templated Porous Bioink

James P. K. Armstrong, Madeline Burke, Benjamin M. Carter, Sean A. Davis, and Adam W. Perriman*

3D cell printing (bioprinting) is rapidly emerging as a key biofabrication strategy for engineering tissue constructs with physiological form and complexity.[1–4] In practice, this process involves layer-by-layer deposition of a cell-laden bioink resulting in the additive manufacture of a patterned architecture with different cell types, growth factors, or mechanical cues, which are positioned with far greater precision than can be achieved with conventional scaffold-based tissue engineering.[5] While there have been significant advances in printing technology,[6,7] progress has been limited by the rate of development of bioinks that are compatible with both 3D printing and tissue engineering.[8] These materials must be able to withstand extrusion, maintain structural fidelity for long time periods, and permit adequate nutrient diffusion, all under cytocompatible conditions. Due to their intrinsic porosity and capacity for high nutrient loading, hydrogels are the most promising candidate for bioink design,[9] particularly when gelation can be externally triggered using chemical bonding,[10] photoinduced crosslinking,[11] thermal setting,[12] or shear-thinning.[13] However, integrating these factors into a system while maintaining printability, structural persistence, and cell viability, is an enduring challenge.[14]

Pluronic block copolymers of poly(ethylene oxide-b-propylene oxide-b-ethylene oxide) present a possible pathway to print gelation, as they undergo a sol–gel transition upon heating near physiological temperatures. Here, elevating the temperature of these non-ionic surfactants reduces the critical micelle concentration (CMC) and increases the micelle volume fraction ($\varnothing_m$), which in turn exceeds the critical limit ($\varnothing_m > 0.53$) resulting in micellar crystallization and formation of a self-supporting gel phase.[12] This phase behavior makes Pluronics ideal for patterning structures during 3D printing; however, their application as cell-supporting bioinks is severely limited by the temperature and concentration dependence of the sol–gel transition, which results in rapid degradation of the printed structure upon cooling or immersion. Accordingly, single-component Pluronic gels are not used to print persistent cellularized structures, instead they have found application as cell-free "fugitive inks" for vascularized scaffold formation.[15]

Conversely, chemically crosslinked gel systems offer excellent structural fidelity in aqueous solutions, but can be limited by poor compatibility with fiber extrusion and layer-by-layer printing. For example, the linear polysaccharide alginate, found naturally in the cell walls of brown algae, can be rapidly crosslinked through chelation of divalent cations by the carboxylic acid groups founds on adjacent strands of the component β-D-mannuronate or α-L-guluronate epimers.[16] Moreover, ionic crosslinking can be achieved using a wide range of readily available salts (of Zn^{2+}, Ni^{2+}, Co^{2+}, Ca^{2+}, Ba^{2+}, Sr^{2+}, etc.), and has been widely exploited to create persistent cell-laden gels for long-term culture and tissue engineering.[17] Unfortunately, the rapid rate of crosslinking prevents effective interlayer adhesion during layer-by-layer immersion printing, and the limited shear thinning capacity during extrusion restricts formulations to low weight percentage alginate gels that exhibit poor mechanical strength and nonviscoelastic rheological properties. Accordingly, the use of alginate gels in 3D bioprinting has been limited to structurally simple objects with limited vertical size, which severely limits their application in tissue printing.[18]

The emergence of hybrid multicomponent gels that integrate desirable physical properties from each constituent component represents an exciting new direction in bioink development. For instance, biodegradable polymers are commonly strengthened with osteoinductive ceramics, such as calcium phosphate,[19] nanofibrous cellulose has been used to increase the shear thinning of alginate gels,[20] while a mixture of Pluronic and acrylated Pluronic has been used to generate a synthetic gel that can be crosslinked using both temperature and ultraviolet irradiation.[21] While these hybrid systems report printability and short-term cytocompatibility (4–14 d), they have not demonstrated practical applicability over a long-term, tissue engineering course. Here, we report on the rational design of a novel Pluronic–alginate multicomponent bioink with complex phase behavior, which was used in a two-step 3D printing process to engineer bone and cartilage architectures. Specifically, 3D structures containing human mesenchymal stem cells

Dr. J. P. K. Armstrong,[+] M. Burke, B. M. Carter,
Dr. A. W. Perriman
School of Cellular and Molecular Medicine
University of Bristol
Bristol BS8 1TD, UK
E-mail: chawp@bristol.ac.uk
M. Burke, Dr. S. A. Davis, Dr. A. W. Perriman
Centre for Organized Matter Chemistry and
Centre for Protolife Research
School of Chemistry
University of Bristol
Bristol BS8 1TS, UK
M. Burke
Bristol Centre for Functional Nanomaterials
University of Bristol
Bristol BS8 1FD, UK
[+]Present address: Department of Materials, Imperial College London, London SW7 2AZ, UK

ADVANCED
HEALTHCARE
MATERIALS
www.advhealthmat.de

Materials Views
www.MaterialsViews.com

COMMUNICATION

(hMSCs) were printed by extruding the shear-thinning, cell-laden gel onto a heated stage, resulting in instantaneous solidification via the sol–gel transition of the Pluronic, and the structures were then stabilized through alginate crosslinking using $CaCl_2$ immersion. The Pluronic constituent also served as a sacrificial template, being completely expelled during crosslinking, which drove the formation of micron-sized pores or anisotropic microchannels. Moreover, the Pluronic-templated alginate gel exhibited favorable biomaterial properties, including increased shear thinning, compressive modulus, and shear modulus. This provided a platform for printing macroscopic structures (ear, nose, tracheal cartilage ring), as well as fine fibers and meshes. Significantly, hMSC-laden 3D architectures showed no significant loss in cell viability over 10 d, and the encapsulated cells could be differentiated into osteoblasts and chondrocytes to engineer printed tissue constructs over five weeks, including a full-size tracheal cartilage ring.

The cellularized bioink was formulated using sodium alginate (alginate) and Pluronic F127 (F127) (**Figure** 1a–c), which involved developing a new methodology to meet the conflicting conditions required to solubilize the separate gel components, retain cell viability, and maintain sterility (see the Experimental Section). Briefly, autoclaved 40 wt% F127 and UV-sterilized 10 wt% sodium alginate were mixed at 4 °C and then at 25 °C, to create a homogenous fluid which could be loaded with hMSCs. A MendelMax 2.0 3D printer retro-fitted with a syringe pump was used to extrude the pre-gelled fluid onto a heated stage set to 37 °C. The elevated temperature instigated a spontaneous sol–gel transition mediated by the F127 component of the printed layers, allowing the generation of self-supporting 3D geometries, which were further stabilized by crosslinking the alginate chains with a $CaCl_2$ wash. Hollow square-based rectangular prisms with outer dimensions of

10 mm × 10 mm × 2.4 mm and a wall thickness of 1.6 mm were printed from six 400-µm thick layers, and this structural template was used to enable high-throughput printing and facile assessment of print quality and structural fidelity (Figure 1d,e).

The 3D printing compatibility of the bioink was tested over a range of F127 concentrations (11, 13, and 15 wt%) at both 5 and 6 wt% sodium alginate. Optimum printing performance was observed using 13 wt% F127 with 6 wt% sodium alginate, which produced reliably smooth prints with reproducible geometries (Figure S1b,e, Supporting Information). Lower F127 content bioinks (11 wt%) did not gel successfully, leading to a collapsed structure with significant spreading at the four corners of the printed construct (Figure S1a,d, Supporting Information), while higher F127 formulations (15 wt%) produced much thicker gels resulting in a "castled" structure with accumulated deposits in the four corners of the printed structure (Figure S1c,f, Supporting Information). While the F127 component was the principle determinant of initial print quality, the alginate constituent allowed post-printing calcium crosslinking for prolonged stability in cell culture media. Accordingly, the sodium alginate concentration was varied between 2 and 6 wt% in formulations containing 13 wt% F127, crosslinked for 10 min in cell medium supplemented with 100×10^{-3} M $CaCl_2$, and then incubated in cell medium for 5 d. The hybrid gel prints containing 2 wt% and 4 wt% alginate had disintegrated at 48 and 120 h, respectively (Figure S2a,b, Supporting Information). Significantly, the hybrid gel structures containing 6 wt% alginate exhibited a retained geometry up to 5 d, after which, the printed structures deformed, lost definition, and disintegrated (Figure S2c, Supporting Information).

The loss of structural fidelity of the printed constructs after 5 d appeared to be largely independent of the $CaCl_2$ concentration used during crosslinking (between 5 and 100×10^{-3} M; Figure S3, Supporting Information). Rather, disintegration was attributed to the higher ionic strength within the gel compared to the surrounding cell medium, which led to osmotic swelling of the printed structure and the displacement of the chelated calcium ions.[22] This hypothesis was supported by an observed increase in the concentration of calcium ions (1×10^{-3} M over 4 h) in cell media containing a single crosslinked structure (Figure S4, Supporting Information). To counter the effect of calcium efflux, the printed structures were incubated in cell media supplemented with millimolar quantities of $CaCl_2$. Here, low levels of $CaCl_2$ ($<3 \times 10^{-3}$ M) failed to preserve the structure of the prints after 10 d (Figure S5a–c, Supporting Information), however, supplementing the media with 5 or 10×10^{-3} M $CaCl_2$ gave excellent structural fidelity (Figure S5d,e, Supporting Information). In summary, the bioink optimization experiments led to a standard protocol whereby 13 wt% F127–6 wt% alginate was crosslinked in $CaCl_2$ for 10 min,
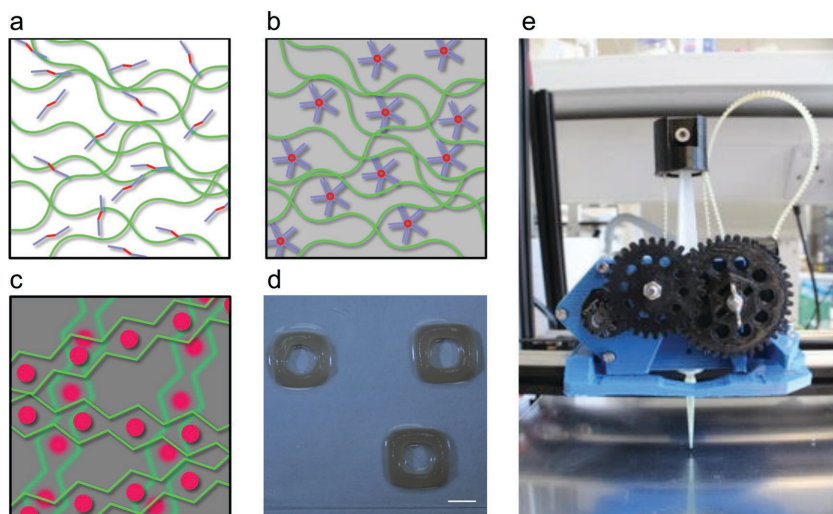

Figure 1. 3D printing using the F127–alginate hybrid gel. a) Pre-printing, the bioink comprises F127 surfactant (blue/red), with a low micelle volume fraction ($\varnothing_m$), and alginate chains (green). b) The elevated temperature of the heated stage reduces the CMC of F127, raising the $\varnothing_m$, and effectively gelling the printed bioink. c) The printed structure is then immersed in $CaCl_2$, which crosslinks the alginate chains, and then washed to fully remove the F127. d) Photographs of a series of hollow square-based prisms, 3D printed using the 13 wt% F127–6 wt% alginate hybrid gel (scale bar = 5 mm). e) The modified MendelMax 2.0 3D printer, fitted with an extruder head for printing with gel-loaded syringes.

Materials
Views
www.MaterialsViews.com

ADVANCED
HEALTHCARE
MATERIALS
www.advhealthmat.de

COMMUNICATION

with a 5×10^{-3} M CaCl$_2$ media supplement used to maintain the structure during long-term culture.

After printing, calcium crosslinking and washing steps were performed at room temperature to allow the F127 to dissolve and diffuse out of the printed gel structure. This dynamic process was monitored using Fourier transform infrared (FTIR) spectroscopy, which was used to track the changes in the transmission bands associated with the mannuronate and guluronate monomers of alginate (for instance, carboxylate stretches at 1411 and 1604 cm^{-1}) and the repeat ether moiety in F127 (prominent stretches at 1103 and 2885 cm^{-1}) (Figure S6, Supporting Information). Significantly, the uncrosslinked hybrid gel possessed a composite spectrum with transmission peaks originating from both components, while the FTIR trace from the post-crosslinked structure was identical to sodium alginate alone. This was consistent with complete expulsion of the F127 component from the hybrid gel leaving behind a macroscopically templated alginate print. Optical microscopy performed on sections stained with the carbohydrate dye Safranin O showed alginate homogenously distributed throughout the printed construct (Figure S7, Supporting Information).

The effect of F127 expulsion on the micro- and nanostructure of the hybrid gel was investigated by scanning electron microscopy (SEM). Crosslinked gel samples were prepared using critical point drying, an established dehydration technique that preserves the integrity of hydrogels for high-resolution imaging.[23] Significantly, SEM micrographs revealed an extensive porous architecture within the crosslinked gel, with a mean pore diameter (d) of 6.4 ± 0.6 µm that was much larger than those observed in alginate alone (d = 0.76 ± 0.06 µm) (**Figure 2**a–c). Pore size was found to systematically increase with a trend toward larger pore structures in the hybrid gels with more F127 (Figure S8, Supporting Information). This indicated that the F127 not only provided a physical template for macroscopic structure formation, but also acted as a microscopic template where the amphiphilic nature of the surfactant molecule stabilized the formation of the large macropores. Porosity is a critical feature in tissue engineering structures, with large pores shown to increase elastic moduli, enhance nutrient mass transport, and provide interstitial space for extracellular matrix (ECM) deposition.[24,25] Moreover, unidirectional calcium diffusion into the hybrid gel generated aligned channels oriented perpendicular to the gel surface (Figure 2d). This behavior has previously been observed in alginate hybrid gels,[26,27] and is thought to occur when hydrodynamic flow arises from friction between the contracting alginate chains and the bulk solution.[28] Such patterned architectures are highly desirable for tissue engineering applications; for example, anisotropic gel environments are used to guide cellular alignment and microchannel architectures are exploited for enhanced nutrient

mass transport.[29] Conversely, under the same experimental conditions, unidirectional calcium diffusion resulted in alginate gels with an isotropic mesh structure (Figure S8, Supporting Information), which suggests that F127 acts as an interfacial stabilizer during the formation of both large pores and aligned channels.[30]

Rheology and compression testing revealed that the hybrid gel, before and after calcium crosslinking, had physical properties significantly different to the equivalent neat alginate and F127 systems. A shear rate ramp performed on uncrosslinked hybrid gels at printing temperature (T = 25 °C) showed a significant decrease in viscosity with increased shear, producing a flow index (n) of 0.126 ± 0.001, which is indicative of a shear thinning material (n < 1) (Figure S9a, Supporting Information). This behavior was far less pronounced for the 6 wt% alginate system (n = 0.629 ± 0.003), while the 13 wt% F127 showed significant shear thinning, which together suggest that F127 enhances the shear thinning behavior of the hybrid gel. Frequency sweeps measuring the elastic (G') and viscous (G'') contributions to shear modulus (G) at 37 °C revealed that the uncrosslinked hybrid gel was viscoelastic ($G' > G''$, slope in G), in contrast to the uncrosslinked 6 wt% alginate ($G' < G''$) (Figure S9b,c, Supporting Information). Calcium ion crosslinking of the hybrid gel resulted in an order of magnitude increase in the shear modulus, which was attributed to the increased rigidity conferred by the interchain chelation of calcium ions. Indeed, no crossover between G' and G'' was observed at low frequencies, which is consistent with the formation of a persistent rigid gel network. Significantly, the crosslinked hybrid gel exhibited a shear modulus approximately
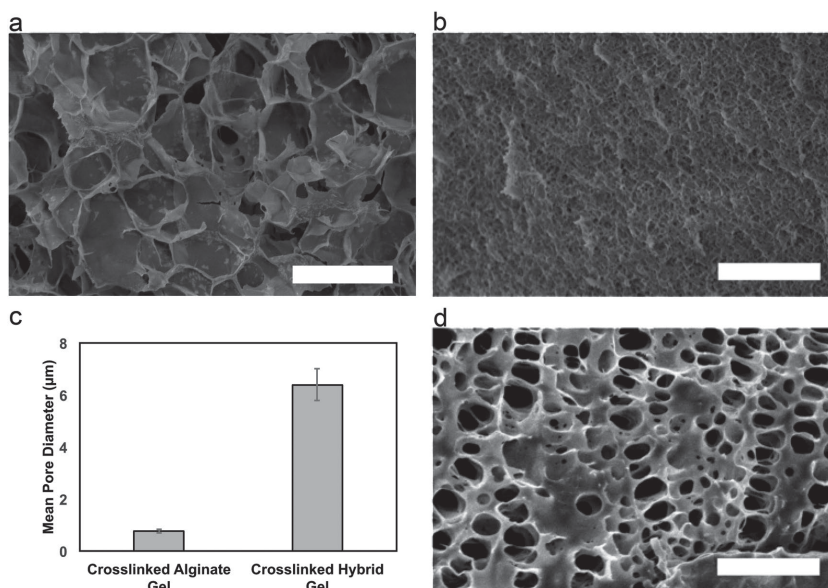

Figure 2. Scanning electron micrographs of the porous structures formed by calcium crosslinking a) 13 wt% F127–6 wt% alginate hybrid gel and b) 6 wt% alginate gel. The hybrid gel exhibited templated macropores that were larger than those observed in the neat alginate gel. c) Semiquantitative image analysis of the micrographs revealed an eightfold increase in mean pore diameter when F127 was used as a templating component (mean and standard deviation reported from 50 measurements). d) Scanning electron microscopy performed on a unidirectionally crosslinked hybrid gel revealed an aligned microchannel structure, that was not observed in the single-component alginate gel (see Figure S8, Supporting Information) (scale bar in all SEM images = 20 µm).

COMMUNICATION

twice that of crosslinked 6 wt% alginate. Furthermore, a strain sweep of the crosslinked hybrid gel showed a linear viscoelastic (LVE) region extending to ≈0.7% of the complex shear strain at 37 °C, which was an order of magnitude larger than the limit measured for crosslinked 6 wt% alginate (≈0.06%) (Figure S9d,e, Supporting Information). Finally, unconfined compression testing at 37 °C gave a Young's modulus (E) of 45 ± 4 kPa for the crosslinked hybrid gel (Figure S9f, Supporting Information), a value that was 50% higher than crosslinked 6 wt% alginate (E = 30 ± 5 kPa) and similar to soft tissues such as articular surface hyaline cartilage (E = 79 ± 39 kPa, as measured in bovine tissue).[31] Taken together, it was evident that the presence of F127 enhanced the shear thinning and rheological characteristics of the uncrosslinked bioink (n, G', G''), while the structural templating significantly improved the rheological and mechanical properties of the final crosslinked construct (E, G', G'', and LVE region).

In light of the favorable mechanical properties and high porosity of the hybrid gel, an array of anatomical structures were printed, including a tracheal cartilage ring, a nose, and an ear (**Figure 3**a,b). The geometry of these printed structures was faithful to the input design; moreover, the final print height of the nose (17.2 mm) demonstrated that the thermally induced sol–gel transition could be propagated effectively through the structure over a large distance from the heated bed. In addition to these macroscopic structures, the hybrid gel was used to print fine crosshatched meshes with a mean voxel area of 0.17 ± 0.03 mm² (Figure 3c). This demonstrated how the resolution could be modified simply by tuning the internal diameter (Ø) of the extrusion tip. For example, a mean line width of 0.69 ± 0.04 mm was achieved using a standard micropipette tip (Ø = 0.50 mm) (Figure 3d), which reduced to 0.41 ± 0.05 mm

in the crosshatch pattern by using a 25-gauge syringe needle (Ø = 0.26 mm), and a mean line width of 0.19 ± 0.01 mm was attained using a 30-gauge syringe needle (Ø = 0.16 mm) (Figure 3e). Taking the average diameter of an adult hMSC to be ≈10–20 µm, these results demonstrate the potential of the hybrid gel for high resolution cell patterning. Moreover, high magnification fluorescence imaging of extruded bioink revealed alignment of the gel fibers parallel to the print vector, which was attributed to shear flow alignment during extrusion (Figure 3f).

A time course study was performed to analyze whether cell loading affected the printing process or structural fidelity of the hybrid gel construct. Significantly, the addition of 3 × 10⁶ cells mL⁻¹ hMSCs to the hybrid gel prior to printing produced no observable effect on extrusion efficacy or structural retention of square prints over the course of 5 d in culture with cell medium (Figure S10, Supporting Information). The viability of the encapsulated hMSCs was assessed over a one-week period using live/dead staining, with confocal fluorescence microscopy and image analysis giving a cell viability of 87% ± 4% (immediately after printing), 79% ± 8% (1 d), 76% ± 3% (2 d), 88% ± 2% (3 d), 81% ± 6% (4 d), and 83% ± 6% (7 d) (Figure S11, Supporting Information). Moreover, cell death from flow-induced shear forces was not evident even at high-resolution prints (23-gauge needle, Ø = 0.34 mm), which gave a post-print cell viability of 83% (Figure S12a, Supporting Information). Low magnification widefield fluorescence microscopy performed on cell-laden square prints allowed clear visualization of the hMSC distribution, with negligible cytotoxicity observed either post-printing or after 10 d in culture in serum-containing cell media (Figure S12b,c, Supporting Information). Previous studies have shown cytotoxic effects when F127 is used as an encapsulating gel (60%–70% viability for 15.6 wt% F127), but not when used as a liquid additive (80%–90% viability for 10 wt% F127), with more severe effects at higher weight percentage and longer exposure time (quoted figures for HepG2 cells, t = 1 d).[32] These values correlate well with the results from our study, where hMSCs are only exposed to 13 wt% F127 during mixing and printing (typically 30–60 min), before F127 is expelled from the hybrid gel. In general, hMSCs encapsulated within the hybrid gel adopted a spherical cell morphology, an equilibrium geometry assumed in the absence of microscale features or integrin binding sites, and typical of nanofibrous gels, such as alginate.[33] Although cells such as chondrocytes and osteoblasts are naturally rounded,[34] an adherent analogue would benefit cells with fibroblastic or neuronal morphology and enable methodological flexibility in printing complex, multiresponsive structures. This could be achieved by introducing cell-binding motifs; for instance, enhanced cell adhesion and spreading has been observed when alginate is covalently tagged with arginylglycylaspartic acid, a tripeptide sequence present in the cellular adhesion protein fibronectin.
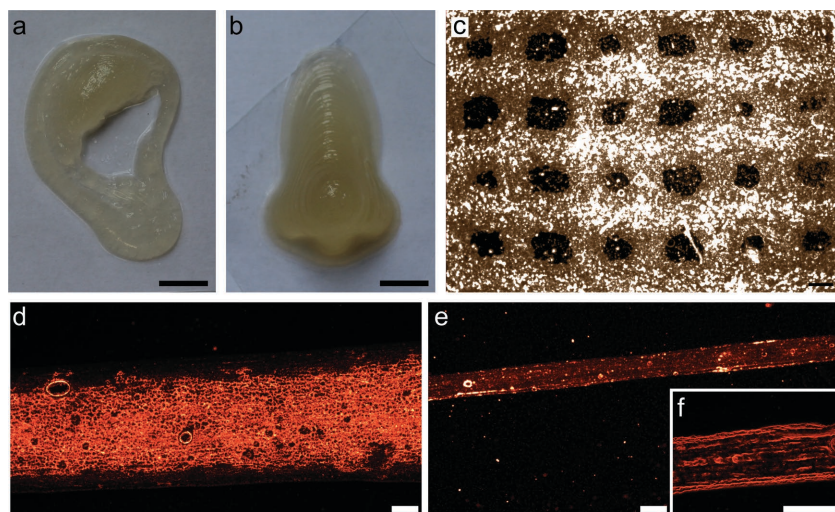

Figure 3. Macro- and microscale 3D printing using the 13 wt% F127–6 wt% alginate hybrid gel. a,b) Post-crosslinking photographs of a full-sized ear and nose, with a height of 0.64 and 1.72 cm, respectively (scale bars = 1 cm). Widefield fluorescence microscopy performed on 3D microstructures printed using the hybrid gel doped with RITC, show c) a crosshatch motif printed through a 25-gauge syringe needle, with an average fiber width of ≈0.41 ± 0.05 mm, d) a single fiber printed through a pipette tip, and e,f) a single fiber printed through a 30-gauge needle. The fiber extruded through large nozzle diameters, such as the pipette tip, displayed no distinguishable anisotropy, whereas the fiber extruded through the needle exhibited significant alignment of the gel in the direction of the print vector (scale bars = 200 µm).
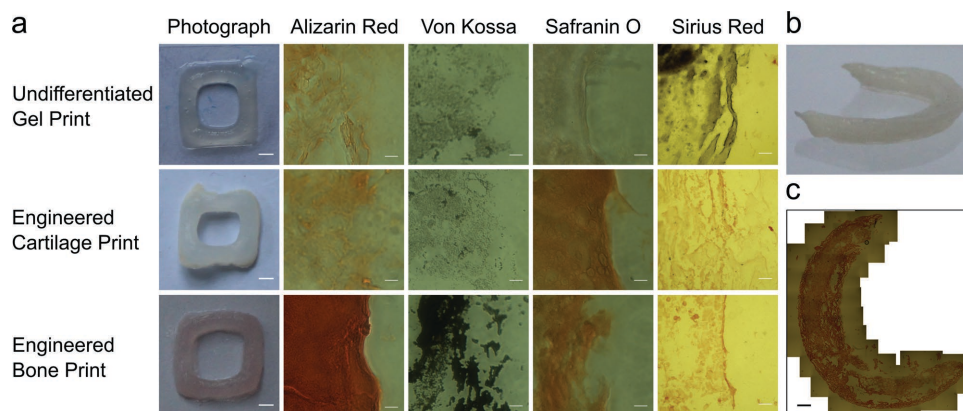
Materials Views
www.MaterialsViews.com

ADVANCED
HEALTHCARE
MATERIALS
www.advhealthmat.de

COMMUNICATION

Figure 4. Tissue engineering using 3D printed constructs of hMSC-laden 13 wt% F127–6 wt% alginate hybrid gel. a) Printed squares were used to engineer cartilage (35 d course) and bone (21 d course), and compared to a standard square print (day 0). Photographs demonstrated the retention of print geometry during long-term tissue culture (scale bar = 2 mm). Histology performed on sections of square prints (scale bar = 10 μm) cultured with chondrogenic growth factors stained positive for glycosaminoglycan (stained red, Safranin O at pH 2.3 to avoid alginate carboxylate staining) and collagen (stained red, Sirius Red). Similarly, constructs treated with osteogenic supplements exhibited widespread inorganic mineral deposits of calcium (stained red, Alizarin Red) and phosphate (stained black, Von Kossa). A full-size tracheal cartilage ring was 3D printed, which b) retained the printed geometry after 35 d of tissue engineering (maximum length = 17 mm, maximum width = 14.5 mm, thickness = 1.8 mm, height = 1.8 mm, see Figure S13 in the Supporting Information for full input parameters) and c) produced an ECM rich in glycosaminoglycan (stained red, Safranin O) (scale bar = 1 mm).

Together, the observations that hMSCs retain viability for up to 10 d and do not negatively impact the print structure offered the opportunity to test the hybrid gel for tissue engineering. To this end, printed constructs containing a high density of hMSCs (6×10^6 cells mL^{-1}) were treated with growth factors known to induce chondrogenesis (transforming growth factor β3, insulin)[35] or osteogenesis (bone morphogenetic protein 2, β-glycerophosphate).[36] Bone and cartilage tissue engineering was performed for three weeks and five weeks, respectively, with the printed constructs possessing excellent structural fidelity throughout this extended culture period. Moreover, the differentiated cells retained their capacity for ECM production, which was visualized in sectioned constructs using an array of histological stains (**Figure 4**a). For instance, the prints treated with chondrogenic growth factors possessed a matrix rich in glycosaminoglycan and collagen, which was revealed by Safranin O and Sirius Red staining, respectively, while the constructs treated with osteogenic growth factors exhibited widespread inorganic mineral deposition of calcium and phosphate, as visualized using Alizarin Red and Von Kossa staining. In a final demonstration of therapeutic potential, hybrid gel loaded with 6×10^6 hMSCs mL^{-1} was printed in the geometry of a full-size tracheal cartilage ring, crosslinked, and then cultured in chondrogenic differentiation medium. This engineered cartilage tissue exhibited retained hemispherical geometry and a glycosaminoglycan-rich ECM (Figure 4b,c), strong evidence that dynamic 3D tissue printing using the hybrid gel can be used to engineer physiological tissue structures.

In conclusion, the new bioink described herein offers a multitude of advantages for bioprinting, compared to single-component gel systems. We have shown that combining separate specialized, functional components can produce a smart soft biomaterial that can be extruded at high-resolution and effectively crosslinked to produce cytocompatible constructs with long-term structural fidelity. Moreover, by using

F127 as a sacrificial guest, we were able to template both the macroscopic and microscopic structure, producing a porous alginate framework with upgraded mechanical properties and enhanced rheological characteristics. This provided a platform for tissue engineering using cell-laden prints, which resulted in widespread matrix production within a confined geometry, a result that opens up new opportunities for printing tissue constructs with complex physiological structure and represents a significant advance toward the ultimate goal of recapitulating physiological tissue structures in vitro.

Experimental Section

Cell Culture: hMSCs were harvested from the proximal femur bone marrow of osteoarthritic patients undergoing total hip replacement surgery, in full accordance with Bristol Southmead Hospital Research Ethics Committee guidelines (reference #078/01) and having received informed consent from all patients. hMSCs were cultured at 37 °C and 5% carbon dioxide in an "expansion medium" using low glucose Dulbecco's Modified Eagle's Medium (DMEM) supplemented with 100 units mL^{-1} penicillin/100 mg mL^{-1} streptomycin (Sigma Aldrich, UK), 2×10^{-3} M GlutaMAX (Invitrogen, USA), 10% (v/v) foetal bovine serum (FBS), and 5 ng mL^{-1} freshly supplemented basic human fibroblast growth factor (Peprotech, USA). Cells were harvested using Dulbecco's phosphate buffered saline (Sigma Aldrich, UK) and trypsin/ethylenediaminetetraacetic acid solution (Sigma Aldrich, UK) and centrifuged into a pellet. This was resuspended in a small (<50 μL) volume of phenol-free DMEM, and then counted, ready for addition to the bioink.

Bioink Preparation: A 40 wt% stock solution of Pluronic F127 (Sigma Aldrich, UK) in low glucose, phenol-free DMEM (Sigma Aldrich, UK) was autoclaved to 121 °C for 40 min, cooled to 4 °C, and used as a sterile solution for three to four weeks. A fresh 10% stock solution of sodium alginate (Sigma Aldrich, UK) in DMEM was mixed for 30 min at room temperature using a BDC250 overhead stirrer (Caframo, Canada), and then sterilized under UV irradiation for 20 min. These solutions were used to prepare working gel formulations; for instance, a 13 wt% F127–6 wt%

alginate was made by mixing 1.2 g of stock F127, 0.65 g stock alginate, and 0.15 g phenol-free DMEM for 1–2 h at 4 °C and then 10 min at room temperature. For cell printing, the DMEM was excluded at this stage to allow the hMSC suspension to be added after the mixing steps. The cell-loaded or cell-free gels were then transferred to a sterile 5 mL syringe (Terumo Corporation, Japan), which was capped with a Mono-Ject tip caps (covered with parafilm) and then pulse centrifuged to 3000 × g. A micropipette was used to create a small air channel in the gel, allowing the syringe plunger to be inserted, ready for printing.

3D Printing: A MendelMax 2.0 desktop 3D printer (Maker's Tool Works, USA) was assembled and used to print a syringe-based universal paste extruder, designed by Richard Horne and available online under a creative commons licence (Thingiverse #20733). Polyvinyl alcohol was used for the extruder body and acrylonitrile butadiene styrene for the gears. Non-printed parts included a timing belt and pulley (2.5 mm pitch), and a NEMA17 high-torque stepper motor. The paste extruder was mounted on the MendelMax printer, replacing the plastic extruder, and then calibrated in x, y, and z directions and extruder step size. For extrusion, the printer was transferred to a tissue culture hood, wiped clean with 70% ethanol, and then sterilized under UV light for 1 h. Commercial hairspray was used to adhere coverslips to the print bed, which was then heated to 37 °C. The gel-loaded syringes were equipped with a cut pipette tip of 0.5 mm internal diameter (Starlab, UK), fitted to the plastic extruder and secured with the extrusion belt. Structures were printed at an extrusion rate of 600 mm min^{-1} (294 mL min^{-1}), immersed for 10 min in phenol-free DMEM supplemented with 100×10^{-3} M $CaCl_2$, washed with phosphate buffered saline and then cultured under standard conditions, until needed. For higher resolution structures, a reduced extrusion rate (200 mm min^{-1}, 98 mL min^{-1}) and either flat-tip needles (25-gauge or 30-gauge, RS Components, UK) or 23-gauge hypodermic needles (Terumo Corporation, Japan) shortened with a Dremel, were used to print structures that were crosslinked and maintained in 5×10^{-3} M $CaCl_2$. In certain cases, a 0.1% (v/v) doping of 10 mg mL^{-1} rhodamine isothiocyanate (RITC, Sigma Aldrich, UK) was used to visualize extruded fibers using widefield fluorescence microscopy. Photographs were taken using a Canon 1200D DSLR with an 18–55 mm lens. All 3D models in the STereoLithography file format were processed into G-code for layer-by-layer printing using Slic3r software (Open Source, http://slic3r.org). Details of the print models are available in the Supporting Information, including the nose and ear (adapted from Thing:306031 and Thing:105808, respectively), as well as the tracheal cartilage ring, square geometry, and cross-hatch motif (custom designed) (Figure S13, Supporting Information).

Cell Viability Studies: Bioink containing hMSCs (3×10^6 cells mL^{-1}) was extruded into square prints or single lines, which were crosslinked and cultured in expansion medium containing 5×10^{-3} M $CaCl_2$. For imaging, the prints were transferred to a 35-mm diameter Petri dish with glass substrate (MatTek, USA) in phenol-free media supplemented with a commercial live/dead stain (Life Technologies, UK) and 20×10^{-3} M HEPES buffer (Sigma Aldrich, UK). These samples were imaged on either an SP8 confocal fluorescence microscope (Leica, UK) using a 10× objective lens, or a DMI3000 inverted widefield fluorescence microscope (Leica, UK) using a 2.5× objective lens and an excitation filter of 450–490 nm. Cell counting image analysis was performed on confocal fluorescence microscopy images using ImageJ software (NIH, USA).

Tissue Engineering: Bioink containing hMSCs (6×10^6 cells mL^{-1}) was printed (square geometry, trachea), crosslinked, and cultured in a differentiation medium supplemented with 5×10^{-3} M $CaCl_2$. Media and growth factor stocks were prepared as follows: chondrogenic basal medium was prepared using high glucose DMEM (Sigma Aldrich, UK) supplemented with 100 units mL^{-1} penicillin/100 mg mL^{-1} streptomycin, 2×10^{-3} M GlutaMAX (Invitrogen, USA), 1% (v/v) sodium pyruvate (Sigma Aldrich, UK), and 1% (v/v) insulin-transferrin-selenium (Sigma Aldrich, UK); osteogenic basal medium was prepared using α-Minimal Essential Medium (Sigma Aldrich, UK) supplemented with 100 units mL^{-1} penicillin/100 mg mL^{-1} streptomycin, 2×10^{-3} M GlutaMAX (Invitrogen, USA), and 2% FBS (fetal bovine serum); dexamethasone (Sigma Aldrich, UK) was dissolved in ethanol as a 100× solution, then diluted in

chondrogenic basal medium to yield a 100×10^{-6} M stock solution that was filter sterilized; 8...0 $\times 10^{-3}$ M ascorbic acid 2-phosphate (Sigma Aldrich, UK) in deionized water was prepared and filter sterilized; 10 mg mL^{-1} insulin (Sigma Aldrich, UK) in acetic acid (pH 2.0, Sigma Aldrich, UK) was prepared and filter sterilized; 1 M β-glycerophosphate disodium salt hydrate (Sigma Aldrich, UK) in deionized water was prepared and filter sterilized; recombinant human transforming growth factor β3 (TGF β3, R&D Systems, UK) was dissolved in a filter-sterilized 1 mg mL^{-1} solution of bovine serum albumin (BSA, Sigma Aldrich, UK) in 4×10^{-3} M hydrochloric acid (Sigma Aldrich, UK) to yield a 100 µg mL^{-1} stock solution; recombinant human bone morphogenetic protein 2 (BMP 2, Peprotech, UK) was dissolved in a filter-sterilized 1 mg mL^{-1} solution of BSA in 4×10^{-3} M hydrochloric acid (Sigma Aldrich, UK) to yield a 100 µg mL^{-1} stock solution. For bone tissue engineering, prints were cultured in osteogenic basal medium freshly supplemented with 0.1 µL mL^{-1} dexamethasone, 2.5 µL mL^{-1} ascorbic acid 2-phosphate, 10 µL mL^{-1} β-glycerophosphate, and 0.25 µL mL^{-1} BMP 2, with media changes three times a week for three weeks. For cartilage engineering, prints were cultured in chondrogenic basal medium freshly supplemented with 1 µL mL^{-1} dexamethasone, 1 µL mL^{-1} ascorbic acid 2-phosphate, and 1 µL mL^{-1} TGF β3 for five weeks, with media changes three times a week, with the addition of 1 µL mL^{-1} insulin for the final four weeks of tissue engineering.

Histological Analysis: The printed tissue was harvested, photographed, and then fixed in Fixation Buffer (BioLegend, USA) for 2 h, transferred to a 70% (v/v) ethanol solution, and then submitted to Histology Services Unit (University of Bristol), where they were embedded in paraffin, cut into 10 µm sections and affixed to Polysine microscope slides (VWR, UK). Samples were rehydrated using 2 min immersions in xylene, 100% ethanol, 70% (v/v) ethanol, and then deionized water. For calcium staining, slides were immersed in 2% Alizarin Red S (Sigma Aldrich, UK) for 5 min, before excess stain was cleared by dipping the samples 20 times in acetone, in 50:50 acetone:xylene, and then in xylene. For Von Kossa phosphate staining, slides were immersed for 90 min in a 5% solution of silver nitrate (Sigma Aldrich, UK), with the container covered in foil and illuminated from above using a table lamp. The slides were then washed four times with deionized water, immersed for 3 min in 5% sodium thiosulphate (Sigma Aldrich, UK), washed twice with deionized water, and then dehydrated using 2 min immersions in 90% (v/v) ethanol and 100% ethanol. For collagen staining, slides were immersed in 0.1% Sirius Red (Sigma Aldrich, UK) for 1 h at room temperature, briefly washed in two changes of 0.5% (v/v) acetic acid and then dehydrated using 2 min immersions in 70% (v/v) ethanol, 90% (v/v) ethanol, and 100% ethanol. For glycosaminoglycan staining, slides were briefly washed with acetic acid (pH 2.3), stained for 2 min using 0.1% Safranin O (pH 2.3), dipped in 95% (v/v) 20 times, 100% ethanol ten times and then immersed for 2 min in xylene. Alginate staining used a similar protocol, using less acidic solutions of acetic acid and safranin O (both pH 2.9) to allow deprotonation of the carboxylic acid chains. Stained sections were mounted in di-n-butyl phthalate in xylene (Fisher Scientific, UK) and imaged using a DMI300 inverted bright field microscope (Leica, UK) with a 100× oil immersion objective lens.

Fourier Transform Infrared Spectroscopy: Lyophilized samples (crosslinked and uncrosslinked 13 wt% F127–6 wt% alginate hybrid gel, F127 and alginate) were analyzed using a Spectrum One FTIR spectrometer (Perkin Elmer, USA). Data were collected in transmission mode, scanned across a wavenumber range of 600–4200 cm^{-1}, with a blank background subtracted from the measured data.

Rheology: Small amplitude oscillatory measurements were performed on the gels at 37 °C using a Kinexus Pro+ Rheometer (Malvern Instruments, UK). Crosslinked or uncrosslinked samples were added to the rheometer plate, the test geometry (diameter = 20 mm, 4° angle) was lowered to a gap height of 500 µm and any excess hydrogel was discarded. A strain sweep from 0.05% to 10% was carried out at an oscillation frequency of 1 Hz to determine the LVE region. From this, an optimized LVE strain of 0.1% was used during a frequency sweep performed from 0.1 to 10 Hz. The linear region of the frequency sweep was then used to determine the elastic modulus (G′) and the viscous

modulus (G''). Steady state shear measurements were performed at a temperature of 25 °C and a shear rate range of 0.1–10 s^{-1}. Nonlinear regression analysis was performed using the Ostwald-de Waele relationship to calculate the flow index.

Compression Testing: The mechanical behavior of the gels was evaluated using unconfined compression testing under displacement control. Samples of alginate or hybrid gel were washed in 100×10^{-3} M CaCl$_2$ to crosslink the chains and, in the latter case, expel any F127. The diameter and thickness were measured, and the sample was positioned between impermeable plates on an Instron 3343 1 kN single column universal testing machine (Instron, UK), fitted with a 10 N load cell. The test rig was lowered to make contact with the gel, and the load and displacement readings were set to zero. The samples were compressed at a rate of 1 mm min^{-1} until either the maximum displacement of 5 mm was reached or the maximum load of 10 N was exceeded. The load and displacement data were recorded in real time, allowing the compressive modulus to be determined from the linear region of the compression phase.

Scanning Electron Microscopy: Small sections of either the 13 wt% F127–6 wt% alginate hybrid gel or the 6 wt% alginate gel were dehydrated using critical point drying, mounted on stubs and sputter coated with silver using a High Resolution Sputter Coater (Agar Scientific, UK). These samples were imaged using a JSM IT300 Scanning Electron Microscope (Jeol Ltd., Japan). For each gel, pore diameters were evaluated using line and measurement functions in Image J software. Fifty pores were sampled across each micrograph, and were used to calculate the mean average and the standard deviation. Unidirectionally crosslinked samples were prepared by adding the CaCl$_2$ on top of the gel in a microcentrifuge tube (Eppendorf, UK).

Calcium Depletion Measurements: A square print, crosslinked for 10 min in 100×10^{-3} M CaCl$_2$, was immersed in 5 mL phenol-free DMEM. A calcium combined ion selective electrode (VWR, UK), calibrated over the range $0–10 \times 10^{-3}$ M was used to measure the solution concentration of calcium in this solution, with measurements taken every 2 min for 24 h.

Supporting Information

Supporting Information is available from the Wiley Online Library or from the author.

Acknowledgements

[1] B. Derby, *Science* **2012**, *338*, 921.

[2] Y.-J. Seol, J. Y. Park, W. Jeong, T.-H. Kim, S.-Y. Kim, D.-W. Cho, *Biomed. Mater. Res. A* **2014**, *103A*, 1404.

[3] F. Pati, J. Jang, D.-H. Ha, S. W. Kim, J.-W. Rhie, J.-H. Shim, D.-H. Kim, D.-W. Cho, *Nat. Commun.* **2014**, *5*, 3935.

[4] J. Groll, T. Boland, T. Blunk, J. A. Burdick, D. W. Cho, P. D. Dalton, B. Derby, G. Forgacs, Q. Li, V. A. Mironov, L. Moroni, M. Nakamura, W. Shu, S. Takeuchi, G. Vozzi, T. B. Woodfield, T. Xu, J. J. Yoo, J. Malda, *Biofabrication* **2016**, *8*, 013001.

[5] T. Boland, T. Xu, B. Damon, X. Cui, *Biotechnol. J.* **2006**, *1*, 910.

[6] S. Moon, S. K. Hasan, Y. S. Song, F. Xu, H. O. Keles, F. Manzur, S. Mikkilieneni, J. W. Hong, J. Nagatomi, E. Haeggstrom, A. Khademhosseini, U. Demirci, *Tissue Eng., Part C* **2010**, *16*, 157.

[7] J. R. Tumbleston, D. Shirvanyants, N. Ermoshkin, R. Janusziewicz, A. R. Johnson, D. Kelly, K. Chen, R. Pinschmidt, J. P. Rolland, A. Ermoshkin, E. T. Samulski, J. M. Desimone, *Science* **2015**, *347*, 635.

[8] J. H. Y. Chung, S. Naficy, Z. Yue, R. Kapsa, A. Quigley, S. E. Moulton, G. G. Wallace, *Biomater. Sci.* **2013**, *1*, 763.

[9] T. Jungst, W. Smolan, K. Schacht, T. Scheibel, J. Groll, *Chem. Rev.* **2016**, *116*, 1496.

[10] J. A. Rowley, G. Madlambayan, D. J. Mooney, *Biomaterials* **1999**, *20*, 45.

[11] J. W. Nichol, S. T. Koshy, H. Bae, C. M. Hwang, S. Yamanlar, A. Khademhosseini, *Biomaterials* **2010**, *31*, 5536.

[12] B. Jeong, S. W. Kim, Y. H. Bae, *Adv. Drug Delivery Rev.* **2002**, *54*, 37.

[13] C. B. Highley, C. B. Rodell, J. A. Burdick, *Adv. Mater.* **2015**, *27*, 5075.

[14] T. Billiet, M. Vandenhaute, J. Schelfhout, S. Van Vlierberghe, P. Dubruel, *Biomaterials* **2012**, *33*, 6020.

[15] D. B. Kolesky, R. L. Truby, A. S. Gladman, T. A. Busbee, K. A. Homan, J. A. Lewis, *Adv. Mater.* **2014**, *26*, 3124.

[16] R. Russo, M. Malinconico, G. Santagata, *Biomacromolecules* **2007**, *8*, 3193.

[17] C. K. Kuo, P. X. Ma, *Biomaterials* **2001**, *22*, 511.

[18] N. E. Fedorovich, W. Schuurman, H. M. Wijnberg, H.-J. Prins, P. R. van Weeren, J. Malda, J. Alblas, W. J. A. Dhert, *Tissue Eng., Part C* **2012**, *18*, 33.

[19] M. J. Mondrinos, R. Dembzynski, L. Lu, V. K. C. Byrapogu, D. M. Wootton, P. I. Lelkes, J. Zhou, *Biomaterials* **2006**, *27*, 4399.

[20] K. Markstedt, A. Mantas, I. Tournier, H. M. Avila, D. Hagg, P. Gatenholm, *Biomacromolecules* **2015**, *16*, 1489.

[21] M. Müller, J. Becher, M. Schnabelrauch, M. Zenobi-Wong, *Biofabrication* **2015**, *7*, 035006.

[22] C. K. Kuo, P. X. Ma, *J. Biomed. Mater. Res., Part A* **2008**, *84*, 899.

[23] A. Boyde, *Scanning Electron Microsc.* **1978**, *2*, 303.

[24] J. Zeltinger, J. K. Sherwood, D. A. Graham, R. Müeller, L. G. Griffith, *Tissue Eng.* **2001**, *7*, 557.

[25] A. A. Al-Munajjed, M. Hien, R. Kujat, J. P. Gleeson, J. Hammer, *J. Mater. Sci.: Mater. Med.* **2008**, *19*, 2859.

[26] F. Despang, A. Borner, R. Dittrich, G. Tomandl, W. Pompe, M. Gelinsky, *Materialwiss. Werkstofftech.* **2005**, *36*, 761.

[27] A. Bernhardt, F. Despang, A. Lode, A. Demmler, T. Hanke, M. Gelinsky, *J. Tissue Eng. Regener. Med.* **2009**, *3*, 54.

[28] J. Thumbs, H. H. Kohler, *Chem. Phys.* **1996**, *208*, 9.

[29] N. Annabi, J. W. Nichol, X. Zhong, C. Ji, S. Koshy, A. Khademhosseini, F. Dehghani, *Tissue Eng., Part B* **2010**, *16*, 371.

[30] H. Omidian, J. G. Rocca, K. Park, *J. Controlled Release* **2005**, *102*, 3.

[31] R. M. Schnigal, D. Gurskis, A. C. Chen, R. L. Sah, *J. Orthop. Res.* **1997**, *15*, 499.

[32] S. F. Khattak, S. R. Bhatia, S. C. Roberts, *Tissue Eng.* **2005**, *11*, 974.

[33] V. Beachley, X. Wen, *Prog. Polym. Sci.* **2010**, *35*, 868.

[34] J. Glowacki, E. Trepman, J. Folkman, *Exp. Biol. Med.* **1983**, *172*, 93.

[35] J. P. K. Armstrong, R. Shakur, J. P. Horne, S. C. Dickinson, C. T. Armstrong, K. Lau, J. Kadiwala, R. Lowe, A. M. Seddon, S. Mann, J. L. R. Anderson, A. W. Perriman, A. P. Hollander, *Nat. Commun.* **2015**, *6*, 7405.

[36] K. J. L. Burg, S. Porter, J. F. Kellam, *Biomaterials* **2000**, *21*, 2347.